

# Beyond Diagonal RIS: Passive Maximum Ratio Transmission and Interference Nulling Enabler

Hamad Yahya, *Member, IEEE*, Hongyu Li, *Graduate Student Member, IEEE*,  
Matteo Nerini, *Graduate Student Member, IEEE*, Bruno Clerckx, *Fellow, IEEE*,  
and Merouane Debbah, *Fellow, IEEE*

**Abstract**—Beyond diagonal reconfigurable intelligent surfaces (BD-RIS) generalizes and goes beyond conventional diagonal reconfigurable intelligent surfaces (D-RIS) by interconnecting elements to generate beyond diagonal scattering matrices, which significantly strengthen the wireless channels. In this work, we use BD-RIS for passive multiuser beamforming in multiuser multiple-input-single-output (MU-MISO) systems. Specifically, we design the scattering matrix of BD-RIS to either maximize the sum received signal power at the users following maximum ratio transmission (MRT), or to nullify the interference at the users following zero forcing (ZF). To control the BD-RIS circuit topology complexity, we present the scattering matrix designs for the single/group/fully-connected BD-RIS architectures. Furthermore, we investigate uniform/optimized power allocation and ZF precoding at the base station (BS). Numerical results show that BD-RIS improves the interference nulling capability and sum rate with fewer reflecting elements (REs) compared to D-RIS. In addition, at moderate to high signal to noise ratios (SNRs), passive interference nulling reduces the complexity at the BS by relaxing the need for precoding or water-filling power allocation design. Furthermore, the passive MRT with ZF precoding achieves a tight sum rate performance to the joint design considering MU-MISO scenarios with many REs while maintaining low computational complexity and simplifying the channel estimation.

**Index Terms**—Beyond diagonal reconfigurable intelligent surfaces (BD-RIS), multiuser beamforming, maximum ratio transmission (MRT), zero forcing (ZF).

## I. INTRODUCTION

INTELLIGENT surfaces such as reconfigurable intelligent surfaces (RIS), also known as intelligent reflecting surfaces (IRS), are emerging technologies for the sixth generation (6G) mobile networks [1], and have recently been introduced to complement active relays [2], [3]. Unlike active relays, RIS is nearly-passive and noiseless, only powering the controller which alters the electrical properties of the reflecting elements (REs) by controlling the impedances attached to it [4]. Benefiting from its passiveness and reconfigurability, RIS has been recognized as a power-efficient enabler to engineer the wireless channel and enhance the communication performance by

manipulating the phase and amplitude of the impinging signals without active circuitry and radio-frequency (RF) chains [5].

### A. Related Work

RIS technologies have gained significant attention recently due to their potential to enhance the communication performance of wireless systems. Among these technologies, two prominent categories have been intensively investigated in the literature, which are diagonal reconfigurable intelligent surfaces (D-RIS) [6], [7], [8], [9], [10], [11], [12] and beyond diagonal reconfigurable intelligent surfaces (BD-RIS) [13], [14], [15], [16], [17], [18], [19], [20], [21], [22], [23], [24], [25], [26], [27]. While these two categories are often discussed separately, it is important to note that BD-RIS can be viewed as a generalization of D-RIS. In other words, BD-RIS encompasses the characteristics of D-RIS as a special case, offering a broader and more flexible framework for reconfigurable intelligent surfaces. The key limitation in D-RIS is that it manipulates only the phase of the incident signal with  $N$  reconfigurable impedances attached to  $N$  REs making single-connected circuit topology. In contrast, BD-RIS manipulates both the phase and amplitude of the incident signal with a network of reconfigurable impedances that connect the  $N$  REs together [13], [14]. By interconnecting all the REs to each other through  $\frac{N(N+1)}{2}$  reconfigurable impedances, the fully-connected BD-RIS has been proposed, having the highest flexibility yet the highest circuit topology complexity. To balance the performance of the fully-connected BD-RIS with its circuit topology complexity, group-connected BD-RIS is introduced by Shen *et al.* [13]. In this architecture, the REs are divided into  $G$  groups, each with a group size of  $N_G = \frac{N}{G}$  REs. Within each group, the REs are interconnected using  $\frac{N_G(N_G+1)}{2}$  reconfigurable impedances, reducing the total number of reconfigurable impedances to  $\frac{N(N_G+1)}{2}$ . Additionally, graph theory is utilized to design optimal architectures with lower circuit topology complexity such as forest-connected and tree-connected [15].

Focusing on various RIS architectures, in existing literature, beamforming design for both D-RIS [6], [7], [8], [9], [10], [11], [12] and BD-RIS [16], [17], [18], [19], [20], [21], [22], [23], [24], [25], [26], [27] aided multiuser multiple-input-single-output (MU-MISO) systems have been studied and explained in detail below.

**D-RIS:** The authors of [6] minimize the transmit power at the base station (BS) while maintaining a certain signal

Hamad Yahya is with the Department of Electrical Engineering, Khalifa University of Science and Technology, Abu Dhabi 127788, UAE (email: hamad.yahya@ku.ac.ae), he is also with the Department of Electrical and Electronic Engineering, Imperial College London, London SW7 2AZ, U.K.

Hongyu Li, Matteo Nerini and Bruno Clerckx are with the Department of Electrical and Electronic Engineering, Imperial College London, London SW7 2AZ, U.K., (e-mail: {c.li21, m.nerini20, b.clerckx}@imperial.ac.uk).

Merouane Debbah is with the 6G Research Center, Khalifa University of Science and Technology, Abu Dhabi 127788, UAE (email: merouane.debbah@ku.ac.ae)

to interference and noise ratio (SINR) level at the users by jointly optimizing the scattering matrix of D-RIS and the active precoder at the BS using the alternating optimization (AO) algorithm. Similarly, Yang *et al.* [7] achieve the same goal using passive maximum ratio transmission (MRT)/zero forcing (ZF) at the D-RIS while iteratively optimizing the power allocation at the BS. Considering the same setup, the authors of [8] use AO framework to maximize the minimum rate for a better user fairness. The authors of [9] derive a closed-form steering vectors-based multiuser linear precoder to null the known interference and minimize the unknown interference. Jiang *et al.* [10] use the AO framework to design the scattering matrix for interference nulling, achieving maximum degrees-of-freedom with high probability when the number of REs is  $N > 2K(K-1)$ , with  $K$  the number of users. The authors of [11] present a robust gradient-based meta-learning approach without pre-training to design the scattering matrix of the D-RIS and the precoder at the BS. Jangsher *et al.* [12] maximize the sum rate of a wireless unmanned aerial vehicle (UAV) with RIS considering energy efficiency constraints and practical limitations such as phase compensation and imperfect channel state information (CSI).

**BD-RIS:** A joint design for the BD-RIS scattering matrix and BS precoder is considered in [16], [17], [18], [19], [20], unlike [21] which considers a two-stage design. The authors of [16], [17] maximize the sum rate of a multi-sector BD-RIS aided system by transforming the original problem into a multi-block optimization using auxiliary variables and solving it iteratively until convergence. In [18], a unified approach is proposed for various objectives such as energy efficiency maximization, energy consumption minimization and sum rate maximization, while satisfying all constraints on the BD-RIS scattering matrix with additional quality-of-service constraints. In [19], Nerini *et al.* derive a closed-form BD-RIS scattering matrix that maximizes the channel gain of the single-user single-input-single-output (SISO) scenario and the solution is extended to the MU-MISO scenario. Sun *et al.* [20] utilize the Takagi factorization-based symmetric unitary projection and AO to jointly design the BS precoder and the fully-connected BD-RIS scattering matrix. The BS precoder aims to minimize the transmitted power and satisfy certain SINR thresholds at the users, while the BD-RIS scattering matrix aims to maximize the equivalent channel's squared trace magnitude. Fang and Mao [21] consider BD-RIS with group/fully-connected architectures and derive a closed-form BD-RIS scattering matrix to maximize the sum of the users' equivalent channel gains following the gradient decent approach and the singular value decomposition (SVD)-based symmetric unitary projection, while regularized ZF precoding is considered at the BS.

Furthermore, BD-RIS has been investigated in cell-free massive multiple-input-multiple-output (MIMO) [22], and integrated sensing and communication (ISAC) systems [23], [24]. For instance, the authors of [22] employed BD-RIS in simultaneous wireless information and power transfer (SWIPT) systems to improve the wireless power transfer. The authors of [23] jointly optimize the BS linear filter, and precoder, as well as the BD-RIS scattering matrix to maximize the sum rate

while satisfying the sensing requirements. Chen and Mao [24] propose a two-stage design to jointly maximize the sum rate and minimize the largest eigenvalue of the Cramér-Rao bound matrix for multiple sensing targets. While the aforementioned works consider reciprocal impedance networks, non-reciprocal single/group/multi-sector-connected BD-RIS architectures are proposed in [25], [26], [27] by relaxing the symmetry constraint.

## B. Motivations and Contributions

Although a local optimal joint design was proposed in [16], [17], the associated computational complexity of the proposed solution is significant. Therefore, a lower complexity two-stage design is proposed for multiuser systems in [21]. Nonetheless, the focus in [21] is primarily on designing the BD-RIS scattering matrix to maximize the norm of the equivalent channel gains while the inter-user interference is neglected, and thus results in performance loss. Hence, it is more suitable for the point-to-point systems as shown in [28]. Therefore, this article focuses on efficiently and effectively addressing the interference management issue in multiuser systems by exploiting the interference management capability at the BD-RIS. The contributions of this work can be summarized as follows:

- 1) An efficient and low-complexity two-stage design is proposed for the BD-RIS scattering matrix and the BS precoding. Specifically, we analyze the received SINR at stage 1. We then design the BD-RIS scattering matrix to either maximize the sum received signal powers at the users following MRT structure, known as *passive MRT*, or to nullify the interference following ZF structure, known as *passive interference nulling*. The proposed BD-RIS scattering matrix design is general for the single/group/fully-connected BD-RIS architectures.
- 2) Closed-form BD-RIS scattering matrix expressions are presented for the passive MRT following the SVD-based symmetric unitary projection [21], while an efficient AO algorithm is presented for the passive interference nulling. It is found that applying the SVD-based symmetric unitary projection improves the received SINR at stage 1 for the passive MRT.
- 3) For stage 2, we consider uniform/optimized power allocation and ZF precoding at the BS. Specifically, the optimized power allocation aims to maximize the sum rate while the BD-RIS scattering matrix is given. For instance, passive MRT requires optimization to achieve sum rate maximization, meanwhile when the passive interference nulling is adopted at the BD-RIS, water-filling power allocation is applied at the BS. On the other hand, ZF precoding at the BS is proposed for the passive MRT.
- 4) The computational complexity for both stages is analyzed considering the two BD-RIS scattering matrix designs, the three BD-RIS architectures, and the BS processes. In addition, the channel state information requirements for each design are specified. For instance, it is found that the passive MRT eases the channel state information requirements which further simplifies the channel estimation.

- 5) The numerical results show that the BD-RIS enhances the interference nulling capability compared to the D-RIS. For instance, BD-RIS can support more users simultaneously for the same number of REs. Also, the algorithm for BD-RIS converges rapidly with a smaller number of iterations and have a more stable interference nulling regardless of the initialization value.

### C. Article Organization

The rest of the article is organized as follows. Sec. II introduces the system and channel models of the BD-RIS-enabled MU-MISO systems. Sec. III is the BD-RIS scattering matrix design for passive MRT and interference nulling considering single/group/fully-connected BD-RIS architectures. Sec. IV is the BS power allocation/precoding design. Sec. V is the numerical results and discussions. Finally, Sec. VI concludes the article with the main remarks and future work. Interested readers are referred to the MATLAB code for this article which is available on <https://github.com/hmjasm/bd-ris-mrt-null>.

### D. Notations

The notations used throughout the paper are explained as follows. Boldface uppercase and lowercase symbols such as  $\mathbf{X}$  and  $\mathbf{x}$  will denote matrix and column vectors, respectively. The matrix Kronecker product symbol is  $\otimes$ , the matrix Khatri-Rao product is  $\odot$ . The transpose, Hermitian transpose, complex conjugate and Moore-pseudoinverse are denoted by  $(\cdot)^T$ ,  $(\cdot)^H$ ,  $(\cdot)^*$  and  $(\cdot)^\dagger$ . Also,  $(x)^+ = \max(x, 0)$ ,  $\lceil \cdot \rceil$  is the ceiling function,  $\mathbb{E}[\cdot]$  is the statistical expectation,  $\text{Re}[\cdot]$  is the real value of a complex number,  $|\cdot|$  is the absolute value,  $\|\cdot\|_2$  is the  $l^2$  norm,  $\|\cdot\|_F$  is the Frobenius norm,  $\text{Tr}(\cdot)$  is the trace,  $[\mathbf{X}]_{i,j}$  is  $i$ -th row and  $j$ -th column entry in  $\mathbf{X}$ ,  $[\mathbf{X}]_{i:\bar{i},j:\bar{j}}$  extracts the  $i$ -th to  $\bar{i}$ -th rows and  $j$ -th to  $\bar{j}$ -th columns of  $\mathbf{X}$ ,  $[\mathbf{x}]_i$  is  $i$ -th entry in  $\mathbf{x}$ . The identity matrix and zeros vectors are denoted as  $\mathbf{I}$  and  $\mathbf{0}$ , respectively. In addition,  $\mathbf{x} = \text{vec}(\mathbf{X})$  is the matrix vectorization process which concatenate the columns of the matrix in one column vector,  $\mathbf{X} = \text{unvec}(\mathbf{x}, [a, b])$  reshapes the vector to an  $a \times b$  matrix,  $\text{diag}(\mathbf{x})$  is a diagonal matrix with the main diagonal being  $\mathbf{x}$ ,  $\text{blkdiag}(\mathbf{X}_1, \mathbf{X}_2, \dots, \mathbf{X}_G)$  is a  $G \times G$  block matrix with the off-diagonal blocks being  $\mathbf{0}$  and the diagonal blocks being  $\mathbf{X}_1, \mathbf{X}_2, \dots, \mathbf{X}_G$ . The complex normal random variable with a zero mean and  $\sigma^2$  variance is denoted as  $\mathcal{CN}(0, \sigma^2)$ .

## II. SYSTEM AND CHANNEL MODELS

In a downlink MU-MISO system, the BS is equipped with  $K$  transmit antennas to serve  $K$  single antenna users through a BD-RIS with  $N$  REs. The precoded signal vector to be transmitted at the antenna ports of the BS can be expressed as  $\mathbf{x} = \mathbf{P}\mathbf{s}$ , where  $\mathbf{s} \in \mathbb{C}^{K \times 1}$  is the information symbols vector with  $\mathbb{E}[\mathbf{s}\mathbf{s}^H] = \mathbf{I}$ , and the precoding matrix is denoted by  $\mathbf{P} \in \mathbb{C}^{K \times K}$  such that  $\|\mathbf{P}\|_F^2 = P_{\max}$  with  $P_{\max}$  the maximum transmission power at the BS. Let the  $k$ th user be denoted as  $U_k$ ,  $k \in \{1, 2, \dots, K\}$ , the received signal at  $U_k$  is expressed as

$$r_k = \mathbf{h}_k^T \Theta \mathbf{W} \mathbf{x} + n_k \quad (1)$$

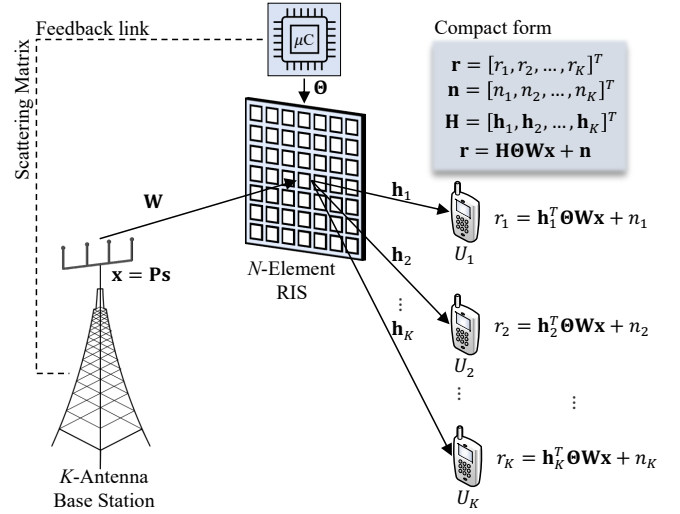


Fig. 1. System block diagram.

where  $\mathbf{W} \in \mathbb{C}^{N \times K}$  is the BS-BD-RIS channel matrix,  $\Theta \in \mathbb{C}^{N \times N}$  is the BD-RIS scattering matrix,  $\mathbf{h}_k \in \mathbb{C}^{N \times 1}$  is BD-RIS- $U_k$  channel vector, and  $n_k \sim \mathcal{CN}(0, N_0)$  is the additive white Gaussian noise (AWGN) with  $N_0$  the power spectral density. It is worth noting that the BS- $U_k$  channel is assumed to be blocked to highlight the performance gain of the BD-RIS [19]. To allow a systematic design of the scattering matrix, (1) can be written in a compact form such that the received signal vector is  $\mathbf{r} = \mathbf{H}\Theta\mathbf{W}\mathbf{x} + \mathbf{n} \in \mathbb{C}^{K \times 1}$ , where  $\mathbf{H} = [\mathbf{h}_1, \dots, \mathbf{h}_K]^T \in \mathbb{C}^{K \times N}$  is the concatenated BD-RIS- $U_k$ ,  $\forall k$  channel matrix, and  $\mathbf{n}$  is the AWGN vector with independent and identically distributed (i.i.d) entries. Fig. 1 depicts the system block diagram.

Depending on the circuit topology for the BD-RIS reconfigurable impedances network, three architectures are considered [13]:

- 1) **Single-connected BD-RIS:** The single-connected BD-RIS is equivalent to the conventional D-RIS. Each RE in this architecture is independently connected with a single grounded reconfigurable impedance without any interconnections among different REs. Consequently, the scattering matrix of the single-connected BD-RIS is a diagonal matrix, which gives rise to the term D-RIS representing the independent operation of each RE. The constraint on the scattering matrix of the single-connected BD-RIS is given as

$$\mathcal{S}_{SC1} = \left\{ \Theta : [\Theta]_{i,j} = 0, \forall i \neq j \right\} \quad (2)$$

where  $i, j \in \{1, 2, \dots, N\}$ . Considering purely reactive impedances, the scattering matrix of the lossless single-connected BD-RIS shall satisfy the unit-modulus constraint for all its elements, i.e.,

$$\mathcal{S}_{SC2} = \left\{ \Theta : |[\Theta]_{i,j}| = 1, \forall i = j \right\} \quad (3)$$

- 2) **Fully-connected BD-RIS:** In the fully-connected BD-RIS architecture, each RE is interconnected with all other REs through a network of reconfigurable impedances, allowing waves impinging on one RE to be reflected by

all other REs. Consequently, the scattering matrix of the fully-connected BD-RIS is a full, reciprocal matrix due to the linearity of the reconfigurable impedances network. Therefore, the symmetry constraint on the scattering matrix of the fully-connected BD-RIS is given as

$$\mathcal{S}_{\text{FC}_1} = \left\{ \Theta : \Theta = \Theta^T \right\} \quad (4)$$

Considering purely reactive impedances, the scattering matrix of the lossless fully-connected BD-RIS shall satisfy the unitary constraint, i.e.,

$$\mathcal{S}_{\text{FC}_2} = \left\{ \Theta : \Theta \Theta^H = \mathbf{I} \right\} \quad (5)$$

- 3) Group-connected BD-RIS: The group-connected BD-RIS architecture divides the REs into  $G$  groups, each with a group size of  $N_G = \frac{N}{G}$  REs. Within each group, the REs are interconnected with all other intra-group REs through a network of reconfigurable impedances, allowing waves impinging on one RE to be reflected by all other intra-group REs only because inter-group REs are disconnected. Consequently, the scattering matrix of the group-connected BD-RIS is a block diagonal, with reciprocal block matrices due to the linearity of the reconfigurable impedances network in each group. Therefore, the symmetry constraint on each block of the scattering matrix of the group-connected BD-RIS is given as

$$\mathcal{S}_{\text{GC}_1} = \left\{ \Theta : \Theta = \text{blkdiag}(\Theta_1, \dots, \Theta_G), \right. \\ \left. \Theta_g = \Theta_g^T, \forall g \right\} \quad (6)$$

where  $\Theta_g \in \mathbb{C}^{N_G \times N_G}$ ,  $g \in \{1, 2, \dots, G\}$ . Considering purely reactive impedances, the scattering matrix of the lossless group-connected BD-RIS shall satisfy the unitary constraint on each block  $\Theta_g$ , i.e.,

$$\mathcal{S}_{\text{GC}_2} = \left\{ \Theta : \Theta_g \Theta_g^H = \mathbf{I}, \forall g \right\} \quad (7)$$

It is worth noting that when  $G = 1$  and  $G = N$ , the group-connected boils down to the fully-connected and single-connected architectures, respectively.

While  $\Theta$  and  $\mathbf{P}$  are given, the received SINR at  $U_k$  is

$$\gamma_k = \frac{|\mathbf{h}_k^T \Theta \mathbf{W} \mathbf{p}_k|^2}{\sum_{i \neq k} |\mathbf{h}_k^T \Theta \mathbf{W} \mathbf{p}_i|^2 + N_0} \quad (8)$$

Consequently, sum rate maximization problem is formulated as

$$(P1) : \max_{\mathbf{P}, \Theta} \sum_k \log_2(1 + \gamma_k) \quad (9a)$$

$$\text{Subject to,} \quad \|\mathbf{P}\|_F^2 = P_{\max} \quad (9b)$$

$$\Theta \in \mathcal{S}_{c_1} \quad (9c)$$

$$\Theta \in \mathcal{S}_{c_2} \quad (9d)$$

where  $c \in \{\text{SC}, \text{FC}, \text{GC}\}$ . The objective function shown in (9a) is non-convex and shows a strong coupling between the precoding matrix and the scattering matrix, which makes

it difficult to jointly optimize the two matrices. The constraint shown in (9b) is non-convex. The constraint shown in (9c) stems from the BD-RIS circuit topology, which is non-convex in general. The constraint shown in (9d) is non-convex [17], and it stems from the lossless nature of the BD-RIS. It is widely known as the Stiefel manifold condition [18]. Therefore, it is suggested to have a two-stage design to decouple the two optimization variables. Unlike [21], our proposed design directly enhances the SINR by applying passive MRT/interference nulling at the BD-RIS. Such approach is motivated by the fact that utilizing ZF solely at the BS usually incurs power penalty because most of the power is wasted for channel inversion, resulting in having very small power gains [29]. Hence, due to the BD-RIS passive nature, enhancing the SINR by the BD-RIS is more effective than relying solely on the BS for precoding.

### III. STAGE 1: BD-RIS SCATTERING MATRIX DESIGN

To explore to what extent BD-RIS could help to enhance the sum rate performance in (9a), we fix the impact of the BS precoding by setting  $\mathbf{P} = \sqrt{p_k} \mathbf{I}$ , where  $p_k = \frac{P_{\max}}{K}, \forall k$ . Hence, the received signal vector can be written as

$$\mathbf{r} = \sqrt{p_k} \mathbf{H} \Theta \mathbf{W} \mathbf{s} + \mathbf{n} \triangleq \sqrt{p_k} \mathbf{H} \Omega \mathbf{s} + \mathbf{n} \triangleq \sqrt{p_k} \mathbf{E} \mathbf{s} + \mathbf{n} \quad (10)$$

where  $\Omega = \Theta \mathbf{W} = [\omega_1, \dots, \omega_K] \in \mathbb{C}^{N \times K}$  and the equivalent channel is  $\mathbf{E} = \mathbf{H} \Omega = [\mathbf{e}_1, \dots, \mathbf{e}_K]^T \in \mathbb{C}^{K \times K}$ . Consequently, the received SINR at  $U_k$  stage 1 is given as

$$\gamma_k = \frac{p_k |\mathbf{h}_k^T \omega_k|^2}{p_k \sum_{i \neq k} |\mathbf{h}_k^T \omega_i|^2 + N_0} = \frac{p_k |[\mathbf{e}_k]_k|^2}{p_k \sum_{i \neq k} |[\mathbf{e}_k]_i|^2 + N_0} \quad (11)$$

Considering (11), the rate at  $U_k$  is influenced by the signal power that is determined by the numerator, as well as the interference which is determined by the summation in the denominator. Therefore, two objectives for the BD-RIS are motivated:

- 1) To maximize the desired signal power.
- 2) To nullify the interference.

The BD-RIS scattering matrix design following the first objective is called *passive MRT*, while the design following the latter is called *passive interference nulling*. It is worth noting that maximizing  $\|\mathbf{E}\|_F^2$  as in [21] would maximize  $\sum_k \sum_i |[\mathbf{e}_k]_i|^2$ . Hence, the numerator and denominator of (11) are maximized simultaneously, which does not necessarily lead to the maximization of the SINR in a MU-MISO setting.

#### A. Passive MRT

To maximize the desired signal power at all users simultaneously, the diagonal elements of  $\mathbf{E}$  need to be considered, i.e.,  $[\mathbf{e}_k]_k$ . Following the approach in [30], it is noted that  $\omega_k$  and  $\exp(j\theta_k) \omega_k$  for any common phase rotation  $\theta_k \in \mathbb{R}$  lead to the same values of  $|[\mathbf{e}_k]_k|$ . Hence, the phase ambiguity can be exploited to make the inner product  $\mathbf{h}_k^T \omega_k$  real and positive without loss of optimality. This motivates us to maximize the real part of  $\mathbf{h}_k^T \omega_k$  instead of its absolute value. Therefore, to capture the desired signal at all users, the trace of the real-valued equivalent channel will be used while relaxing the

challenging constraints in (9c) and (9d). Consequently, we can find a relaxed  $\Theta$  by solving the following problem

$$(P2a) : \max_{\Theta} f(\Theta) \triangleq \text{Tr}(\text{Re}[\mathbf{E}]) = \text{Tr}(\text{Re}[\mathbf{H}\Theta\mathbf{W}]) \quad (12a)$$

$$\text{Subject to, } \|\Theta\|_F^2 = N \quad (12b)$$

The objective function can be written as  $f(\Theta) = \text{Tr}(\text{Re}[\mathbf{E}]) = \frac{1}{2}(\text{Tr}(\mathbf{E}) + \text{Tr}(\mathbf{E}^*)) = \frac{1}{2}(\text{Tr}(\mathbf{E}) + \text{Tr}(\mathbf{E}^*)) = \text{Re}[\text{Tr}(\mathbf{E})]$ . Hence,  $f(\Theta) = \text{Tr}(\text{Re}[\mathbf{H}\Theta\mathbf{W}]) = \text{Re}[\text{Tr}(\mathbf{H}\Theta\mathbf{W})]$ . Using the cyclic property of the trace, we can write the objective function in (12a) as  $f(\Theta) = \text{Re}[\text{Tr}(\mathbf{G}\Theta)]$ , where  $\mathbf{G} = \mathbf{W}\mathbf{H} \in \mathbb{C}^{N \times N}$  is the cascaded BS-BD-RIS- $U_k$  channel matrix. In the following, we outline the passive MRT solution for the single-connected and group-connected BD-RIS architectures, where the latter captures the fully-connected architecture as well.

1) *Solution for Single-Connected BD-RIS*: While noting that the single-connected architecture has a diagonal  $\Theta$  with unit modulus elements, we can expand (P2a) as

$$(P2a) : \max_{\Theta} f(\Theta) = \text{Re} \left[ \sum_{i=1}^N [\mathbf{G}]_{i,i} [\Theta]_{i,i} \right] \quad (13a)$$

$$\text{Subject to, } \sum_{i=1}^N |[\Theta]_{i,i}|^2 = N \quad (13b)$$

Therefore, the optimal scattering matrix that belongs to the feasible set, i.e.,  $\mathcal{S}_{\text{SC}_1}$  and  $\mathcal{S}_{\text{SC}_2}$ , is given as

$$[\Theta^*]_{i,j} = \begin{cases} \Pi_{\mathcal{S}_{\text{unim}}}([\mathbf{G}]_{i,j}^*), & i = j \\ 0, & i \neq j \end{cases} \quad (14)$$

where

$$\Pi_{\mathcal{S}_{\text{unim}}}([\mathbf{G}]_{i,j}^*) = \frac{[\mathbf{G}]_{i,j}^*}{|[\mathbf{G}]_{i,j}^*|} \quad (15)$$

is the projection to the unit-modulus constraint shown in (3) with the minimum Euclidean distance to  $[\mathbf{G}]_{i,j}^*$  [10].

*Computational Complexity*: The computational complexity of (14) depends on the computational complexity of computing the diagonal elements of  $\mathbf{G}^*$ ,  $\mathcal{O}(KN)$ , while the normalization has a computational complexity  $\mathcal{O}(N)$ . Hence, the overall complexity can be written as  $\mathcal{O}(KN + N) = \mathcal{O}(KN)$ .

2) *Solution for Group-Connected BD-RIS*: While noting that the group-connected architecture has a block diagonal  $\Theta$  with unitary  $\Theta_g$ , we define  $\mathbf{G}_g \triangleq [\mathbf{G}]_{N_g(g-1)+1:N_g, N_g(g-1)+1:N_g} \in \mathbb{C}^{N_g \times N_g}$ . Hence, we can expand (P2a) as

$$(P2a) : \max_{\Theta} f(\Theta) = \text{Re} \left[ \sum_{g=1}^G \sum_{i=1}^{N_g} \sum_{j=1}^{N_g} [\mathbf{G}_g]_{i,j} [\Theta_g]_{j,i} \right] \quad (16a)$$

$$\text{Subject to, } \sum_{i=1}^{N_g} \sum_{j=1}^{N_g} |[\Theta_g]_{j,i}|^2 = N_g, \forall g \quad (16b)$$

Consequently, the objective function in (16a) can be maximized by co-phasing the terms  $[\mathbf{G}_g]_{i,j}$  and  $[\Theta_g]_{j,i}$  before

summation. Such problem has a closed-form solution that follows the MRT precoding [31] and the pseudo match-and-forward precoding for non-regenerative MIMO relays [32]. Consequently, the closed-form solution given as

$$\Theta = \text{blkdiag}(\Theta_1, \dots, \Theta_G)$$

$$\Theta_g = \mathbf{G}_g^H \sqrt{\frac{N_g}{\text{Tr}(\mathbf{G}_g \mathbf{G}_g^H)}} \quad (17)$$

Since (17) does not belong to the feasible set, i.e.,  $\mathcal{S}_{\text{GC}_1}$  and  $\mathcal{S}_{\text{GC}_2}$ , we project such low-complexity  $\Theta$  to the feasible set using the SVD-based symmetric unitary projection. In other words, we formulate an optimization problem to find  $\Theta$  which belongs to the feasible set by minimizing the squared Frobenius distance between the low-complexity  $\Theta_g$  and the desired  $\Theta_g$ . Hence,

$$(P2b) : \Theta_g^* = \arg \min_{\Theta_g} \left\| \Theta_g - \mathbf{G}_g^H \sqrt{\frac{N_g}{\text{Tr}(\mathbf{G}_g \mathbf{G}_g^H)}} \right\|_F^2 \quad (18a)$$

$$\text{Subject to, (9c), (9d)} \quad (18b)$$

Such approach is known as a matrix approximation and is used due to its ease of computation. In addition, the squared Frobenius norm is used specifically because it is reported that it maximizes the entropy for quantized channels in MIMO systems [33]. This problem can be solved efficiently following [21, Eq. (10)-(12)], which projects the low-complexity solution to the feasible set, i.e., (17) needs symmetric unitary projection. A closed-form symmetric projection of  $\Theta_g$  is given as [21, Eq. (10)],

$$\Pi_{\mathcal{S}_{\text{sym}}}(\Theta_g) = 0.5 (\Theta_g + \Theta_g^T) \quad (19)$$

The unitary projection of  $\Theta_g$  is given as [21, Eq. (11)],

$$\Pi_{\mathcal{S}_{\text{uni}}}(\Theta_g) = \mathbf{U}\mathbf{V}^H \quad (20)$$

where its SVD can be written as  $\Theta_g = \mathbf{U}\Sigma\mathbf{V}^H$ ,  $\mathbf{U}$  and  $\mathbf{V}$  are the unitary left and right singular vectors and  $\Sigma$  contains the singular values ordered in a descending order. Finally, the SVD-based symmetric unitary projection of  $\Theta_g$  is given as [21, Eq. (12)],

$$\Pi_{\mathcal{S}_{\text{symuni}}}(\Theta_g) = \hat{\mathbf{U}}\mathbf{V}^H \quad (21)$$

where  $\Pi_{\mathcal{S}_{\text{sym}}}(\Theta_g)$  is a rank deficient matrix with rank  $R$  and its unitary left and right singular vectors are  $\mathbf{U} = [\mathbf{U}_R, \mathbf{U}_{N-R}]$  and  $\mathbf{V} = [\mathbf{V}_R, \mathbf{V}_{N-R}]$ . Also,  $\hat{\mathbf{U}} = [\mathbf{U}_R, \mathbf{V}_{N-R}^*]$ . Hence, we can express the optimal scattering matrix in closed-form as

$$\Theta^* = \text{blkdiag}(\Theta_1^*, \dots, \Theta_G^*) \quad (22)$$

$$\Theta_g^* = \Pi_{\mathcal{S}_{\text{symuni}}} \left( \mathbf{G}_g^H \sqrt{\frac{N_g}{\text{Tr}(\mathbf{G}_g \mathbf{G}_g^H)}} \right) \quad (23)$$

It should be noted that the signal in general will be degraded due to the SVD-based symmetric unitary projection. It will be seen in the Numerical Results and Discussions Section that the SVD-based symmetric unitary projection not only will degrade the signal power but also will reduce the interference power in (11).

**Computational Complexity:** The computational complexity of (23) depends on the complexity of (17),  $\mathcal{O}(GKN_g^2 + GN_g^2)$ , and is dominated by the  $G$  SVD computations for (21),  $\mathcal{O}(GN_g^3)$ . Hence, the overall complexity can be written as  $\mathcal{O}(GN_g^3 + GKN_g^2 + GN_g^2) = \mathcal{O}(GN_g^3)$ .

**Channel State Information Requirements:** Furthermore, the cascaded BS-BD-RIS- $U_k$  channel matrix,  $\mathbf{G}$ , is needed to compute  $\Theta^*$  for the three architectures. This can be found by selecting the inter-impedance elements of the BD-RIS to have an infinitely large reactance. Hence,  $\mathbf{G}$  can be estimated by setting  $\Theta = \mathbf{I}$  [34]. Therefore, the channel estimation is simplified without separately estimating  $\mathbf{H}$  and  $\mathbf{W}$ .

### B. Passive Interference Nulling

To nullify the interference terms in (11), the equivalent channel should result in a diagonal matrix, i.e.,  $\mathbf{E} = \mathbf{H}\Theta\mathbf{W} = \text{diag}(\lambda)$  and  $\lambda \in \mathbb{C}^{K \times 1}$  is the interference-free equivalent channels at the users. Considering the most flexible architecture which is the fully-connected, an intuitive approach to design a low-complexity  $\Theta$  that nulls the interference follows the ZF precoding. Hence,

$$\Theta = \mathbf{G}^\dagger \sqrt{\frac{N}{\text{Tr}(\mathbf{G}^{\dagger H} \mathbf{G}^\dagger)}} \quad (24)$$

where  $\mathbf{G}^\dagger = \mathbf{H}^H (\mathbf{H}\mathbf{H}^H)^{-1} (\mathbf{W}^H \mathbf{W})^{-1} \mathbf{W}^H$  and the normalization factor is to satisfy the constraint in (12b). Nonetheless, (24) does not belong to the feasible set. Hence, the optimal symmetric unitary scattering matrix that is the closest to (24) in terms of Frobenius norm can be written in closed-form as  $\Theta^* = \Pi_{\mathcal{S}_{\text{symuni}}} \left( \mathbf{G}^\dagger \sqrt{\frac{N}{\text{Tr}(\mathbf{G}^{\dagger H} \mathbf{G}^\dagger)}} \right)$ .

It is worth noting that the approximation error has a determinantal effect on the equivalent channel as  $\mathbf{E}$  will be no longer diagonal which is proved in the following.

*Proof.* While dropping the normalization factor in (24), the equivalent channel can be written as

$$\mathbf{E} = \mathbf{H}\mathbf{H}^\dagger \mathbf{W}^\dagger \mathbf{W} = \mathbf{I} \quad (25)$$

While we consider the symmetry condition alone to facilitate the proof, the equivalent channel becomes

$$\begin{aligned} \hat{\mathbf{E}} &= 0.5\mathbf{H}\mathbf{H}^\dagger \mathbf{W}^\dagger \mathbf{W} + 0.5\mathbf{H}\mathbf{W}^{\dagger T} \mathbf{H}^{\dagger T} \mathbf{W} \\ &= 0.5\mathbf{I} + 0.5\mathbf{H}\mathbf{W}^{\dagger T} \mathbf{H}^{\dagger T} \mathbf{W} \end{aligned} \quad (26)$$

which is in general not a diagonal matrix.  $\square$

To effectively nullify the interference, we adopt an alternative approach as detailed below. The adopted approach is inspired by the interference nulling presented for D-RIS in [10]. Hence, to null the interference in a BD-RIS-enabled MU-MISO system, the equivalent channel, i.e.,  $\mathbf{E}$ , needs to be classified into a desired/interference channels. Then,  $\Theta$  shall be tuned to null all interference channels. In the following, we illustrate interference nulling for the group-connected architecture which captures the fully-connected and single-connected BD-RIS architectures as a special case.

We can re-write the equivalent channel as

$$\text{vec}(\mathbf{E}) = \mathbf{A}_c \theta_c \quad (27)$$

where  $\theta_c \in \mathbb{C}^{GN_g^2 \times 1}$  and is given as

$$\theta_c = \begin{cases} [[\Theta]_{1,1}, [\Theta]_{2,2}, \dots, [\Theta]_{N,N}]^T, & c = \text{SC} \\ \text{vec}(\Theta), & c = \text{FC} \\ [\text{vec}(\Theta_1)^T, \dots, \text{vec}(\Theta_G)^T]^T, & c = \text{GC} \end{cases} \quad (28)$$

$\theta_{\text{SC}} \in \mathbb{C}^{N \times 1}$ ,  $\theta_{\text{FC}} \in \mathbb{C}^{N^2 \times 1}$ ,  $\theta_{\text{GC}} \in \mathbb{C}^{GN_g^2 \times 1}$ ,  $\mathbf{A}_c \in \mathbb{C}^{K^2 \times GN_g^2}$  denotes the desired/interference channels and is given as

$$\mathbf{A}_c = \begin{cases} \mathbf{W}^T \odot \mathbf{H}, & c = \text{SC} \\ \mathbf{W}^T \otimes \mathbf{H}, & c = \text{FC} \\ [\mathbf{W}_1^T \otimes \mathbf{H}_1, \dots, \mathbf{W}_G^T \otimes \mathbf{H}_G], & c = \text{GC} \end{cases} \quad (29)$$

$\mathbf{W}_g = [\mathbf{W}]_{N_g(g-1)+1: gN_g, 1: K} \in \mathbb{C}^{N_g \times K}$ ,  $\mathbf{H}_g = [\mathbf{H}]_{1: K, N_g(g-1)+1: gN_g} \in \mathbb{C}^{K \times N_g}$ ,  $\mathbf{A}_{\text{SC}} \in \mathbb{C}^{K^2 \times N}$ ,  $\mathbf{A}_{\text{FC}} \in \mathbb{C}^{K^2 \times N^2}$ ,  $\mathbf{A}_{\text{GC}} \in \mathbb{C}^{K^2 \times GN_g^2}$ . To define the desired/interference channels, we drop the subscript defining the BD-RIS architecture for notational simplicity. For instance,  $\mathbf{a}_i^T = [\mathbf{A}_c]_{i,:}$  represents the desired/interference channels for a specific user. We define  $\tilde{\mathbf{a}}_{\hat{k},k} = \mathbf{a}_i$ , for  $i = (k-1) \times K + \hat{k}$ . If  $\hat{k} = k$ , then  $\tilde{\mathbf{a}}_{\hat{k},k}$  is the desired channel for  $U_k$ . Otherwise,  $\tilde{\mathbf{a}}_{\hat{k},k}$  is the interference channel for  $U_k$  from antenna  $\hat{k}$ . Consequently, the interference channels matrix can be defined as

$$\bar{\mathbf{A}}_c = [\bar{\mathbf{A}}_1, \bar{\mathbf{A}}_2, \dots, \bar{\mathbf{A}}_K] \in \mathbb{C}^{GN_g^2 \times K(K-1)} \quad (30a)$$

$$\bar{\mathbf{A}}_1 = [\tilde{\mathbf{a}}_{2,1}, \tilde{\mathbf{a}}_{3,1}, \dots, \tilde{\mathbf{a}}_{K,1}] \quad (30b)$$

$$\begin{aligned} \bar{\mathbf{A}}_k &= [\tilde{\mathbf{a}}_{1,k}, \dots, \tilde{\mathbf{a}}_{k-1,k}, \tilde{\mathbf{a}}_{k+1,k}, \dots, \tilde{\mathbf{a}}_{K,k}], \\ &1 < k \leq K-1 \end{aligned} \quad (30c)$$

$$\bar{\mathbf{A}}_K = [\tilde{\mathbf{a}}_{1,K}, \tilde{\mathbf{a}}_{2,K}, \dots, \tilde{\mathbf{a}}_{K-1,K}] \quad (30d)$$

In addition, the desired channels matrix is defined as  $\check{\mathbf{A}}_c = [\tilde{\mathbf{a}}_{1,1}, \tilde{\mathbf{a}}_{2,2}, \dots, \tilde{\mathbf{a}}_{K,K}] \in \mathbb{C}^{GN_g^2 \times K}$ .

To achieve  $\mathbf{E} = \text{diag}(\lambda) \Leftrightarrow \mathbf{A}_c \theta_c = \lambda$ , the  $K(K-1)$  interference channels needs to be nulled by the BD-RIS. This can be achieved by satisfying the nulling condition, which is expressed as

$$\bar{\mathbf{A}}_c^T \theta_c = \mathbf{0} \quad (31)$$

In general, (31) can be seen as a system of linear equations with  $K(K-1)$  complex equations and  $GN_g^2$  complex variables. Nonetheless, the number of effective variables is less due to the constraints on  $\Theta$ , i.e., (9c)–(9d), which is  $\frac{N(1+N_g)}{2}$  real variables. Therefore, given that the channel realizations are random, (31) can be achieved with high probability if the number of real variables is greater or equal the number of real equations, i.e.,

$$\frac{N(1+N_g)}{2} \geq 2K(K-1) \quad (32)$$

which can be solved for  $N$  considering  $K > 1$  as follows

$$\begin{cases} N \geq 2K(K-1), & c = \text{SC} \\ N \geq 2K-1, & c = \text{FC} \\ N \geq \left\lceil \frac{4K(K-1)}{1+N_g} \right\rceil, & c = \text{GC} \end{cases} \quad (33)$$

**Algorithm 1:** AO for passive interference nulling.

---

**Input:**  $\bar{\mathbf{A}}_c$ ,  $G$ , Iter,  $\epsilon$ ,  $\varepsilon$   
**Output:**  $\Theta^*$

- 1 Set  $t = 0$ ; Initialize  $\Theta^{(t)}$ ; Extract  $\theta_c^{(t)}$  (28)
- 2 **if**  $G=1$  **then**
- 3      $[\tilde{\theta}_c^{(t)}]_i = \Pi_{\mathcal{S}_{\text{unim}}}([\theta_c^{(t)}]_i), \forall i \in \{1, 2, \dots, N\}$
- 4      $\tilde{\Theta}^{(t)} = \text{diag}(\tilde{\theta}_c^{(t)})$
- 5 **else**
- 6     **for**  $g = 1 : G$  **do**
- 7          $\Theta_g^{(t)} = \text{unvec}([\theta_c^{(t)}]_{(g-1)N_g^2+1:gN_g^2}, [N_g, N_g])$
- 8          $\tilde{\Theta}_g^{(t)} = \Pi_{\mathcal{S}_{\text{sym}}}(\Pi_{\mathcal{S}_{\text{uni}}}(\Theta_g^{(t)}))$
- 9          $\tilde{\theta}_c^{(t)} = [\text{vec}(\tilde{\Theta}_1^{(t)})^T, \dots, \text{vec}(\tilde{\Theta}_G^{(t)})^T]^T$
- 10         $\tilde{\Theta}^{(t)} = \text{blkdiag}(\tilde{\Theta}_1^{(t)}, \dots, \tilde{\Theta}_G^{(t)})$
- 11 **for**  $t = 1 : \text{Iter}$  **do**
- 12      $\theta_c^{(t)} = \Pi_{\mathcal{S}_{\text{null}}}(\tilde{\theta}_c^{(t-1)})$
- 13     Repeat Lines 2–10
- 14      $\delta = \frac{\|\bar{\mathbf{A}}_c^T \tilde{\theta}_c^{(t)}\|_2^2 - \|\bar{\mathbf{A}}_c^T \tilde{\theta}_c^{(t-1)}\|_2^2}{\|\bar{\mathbf{A}}_c^T \tilde{\theta}_c^{(t-1)}\|_2^2}$
- 15     **if**  $\delta \leq \varepsilon$  **or**  $\|\bar{\mathbf{A}}_c^T \tilde{\theta}_c^{(t)}\|_2^2 < \epsilon$  **or**  $t > \text{Iter}$  **then**
- 16         **break** and **go to** Line 17
- 17  $\Theta^* = \tilde{\Theta}^{(t)}$

---

The expression for the fully-connected architecture can be proved by solving the quadratic inequality and noting that  $K$  and  $N$  are integers, and  $N_g = N$  showing that  $\frac{-1+\sqrt{16K^2-16K+1}}{2}$  lies strictly between  $2K-2$  and  $2K-1$ . Furthermore, (32) can be solved for  $K$  as follows

$$\begin{cases} K \leq \left\lfloor \frac{1+\sqrt{1+2N}}{2} \right\rfloor, & c = \text{SC} \\ K \leq \left\lfloor \frac{N+1}{2} \right\rfloor, & c = \text{FC} \\ K \leq \left\lfloor \frac{1+\sqrt{1+N(1+N_g)}}{2} \right\rfloor, & c = \text{GC} \end{cases} \quad (34)$$

Consequently, the objective is to find  $\Theta$  that is subject to the interference nulling and BD-RIS constraints. In other words, we have the following feasibility-check problem

$$(P3) : \text{Find } \Theta \quad (35a)$$

$$\text{Subject to, (31), (9c), (9d)} \quad (35b)$$

Such problem is non-convex and challenging to solve. Therefore, AO is used to find  $\Theta$  that complies with the previously mentioned constraints by projecting a certain initial solution into  $\mathcal{S}_{\text{null}}$ ,  $\mathcal{S}_{c_1}$  and  $\mathcal{S}_{c_2}$  alternatively. Fortunately, the projections to  $\mathcal{S}_{c_1}$  and  $\mathcal{S}_{c_2}$  have been presented with closed-form solutions in (15), (19)–(20), while the interference nulling projection follows [10, Eq. (21a)] such that

$$\Pi_{\mathcal{S}_{\text{null}}}(\theta_c) = \theta_c - \bar{\mathbf{A}}_c^* (\bar{\mathbf{A}}_c^T \bar{\mathbf{A}}_c)^{-1} \bar{\mathbf{A}}_c^T \theta_c \quad (36)$$

A pseudo-code that illustrates the steps to obtain  $\Theta^*$  through AO is given in Algorithm 1. The algorithm needs the interference channels matrix  $\bar{\mathbf{A}}_c$  and the number of groups  $G$  as inputs. It starts by initializing the scattering matrix, which can be either a random initialization or a specific initialization. In addition, the initialized scattering matrix is projected to  $\mathcal{S}_{c_1}$  and  $\mathcal{S}_{c_2}$  in Lines 2–10. Lines 11–16 illustrate the iterative AO which projects the  $\Theta$  from the previous iteration to interference nulling set and  $\mathcal{S}_{c_1}$  and  $\mathcal{S}_{c_2}$ . This continues for a certain number of iterations until the breaking condition on line 15 is met. On line 14,  $\delta$  is computed which is the  $l^2$  norm for the nulling condition difference between the current iteration and the previous iteration. Finally,  $\Theta^*$  that achieves interference nulling and belongs to  $\mathcal{S}_{c_1}$  and  $\mathcal{S}_{c_2}$  is returned. It is worth noting that  $\epsilon$  and  $\varepsilon$  determine the algorithm convergence speed, where the former is the relative rate of change tolerance and the latter is the nulling condition norm tolerance.

Fig. 2 compares the convergence of Algorithm 1 for fully-connected, group-connected and single-connected BD-RISs. Random initialization is assumed for both, with  $N = 144$ ,  $K = 8$ ,  $\epsilon = 10^{-10}$ ,  $\varepsilon = 10^{-6}$ , Iter =  $10^4$ , and 100 realizations are considered for Monte-Carlo simulation. Also, i.i.d Rayleigh fading channels are considered. The curves represent the average convergence of the algorithm over  $10^4$  iterations, while the shades represent the possible variations, i.e., the maximum and minimum convergence. It can be observed that fully-connected BD-RIS achieves a rapid interference nulling, reaching  $10^{-8}$  with significantly fewer iterations compared to single-connected BD-RIS. In addition, the relative change for the fully-connected BD-RIS stabilizes after fewer iterations compared to the single-connected BD-RIS. Moreover, the fully-connected BD-RIS maintains a stable pattern, effectively achieving interference nulling, unlike the single-connected BD-RIS which is more dependent on the initialization of the scattering matrix, resulting in less stable interference nulling. Furthermore, the behavior of the group-connected BD-RIS falls between the two extremes. Specifically, as the group size approaches  $N$ , the performance becomes closer to that of a fully-connected BD-RIS. Conversely, as the group size approaches 1, the performance becomes similar to that of the single-connected BD-RIS.

**Computational Complexity:** The computational complexity of Algorithm 1 is dominated by computing the projections inside the loop. For instance, in (36), its main part, i.e.,  $\bar{\mathbf{A}}_c^* (\bar{\mathbf{A}}_c^T \bar{\mathbf{A}}_c)^{-1} \bar{\mathbf{A}}_c^T$ , can be computed outside the loop as it only depends on the interference channels matrix. Hence, its computational complexity can be written as  $\mathcal{O}(K^6 + K^4 G N_g^2 + K^2 G^2 N_g^4 + K^2 G N_g^2)$ . For the single-connected architecture, the unit-modulus projection has a computational complexity of  $\mathcal{O}(tN)$ , while the symmetric and unitary projections associated with group-connected architecture have a computational complexity of  $\mathcal{O}(tG N_g^3)$  and  $\mathcal{O}(tG N_g^2)$ . Consequently, the overall algorithm's computational complexity is  $\mathcal{O}(tG N_g^3 + tG N_g^2 + K^6 + K^4 G N_g^2 + K^2 G^2 N_g^4 + K^2 G N_g^2)$ . Typically, when  $N \gg K$  the computational complexity can be written as  $\mathcal{O}(K^2 G^2 N_g^4)$ . Moreover, the Numerical

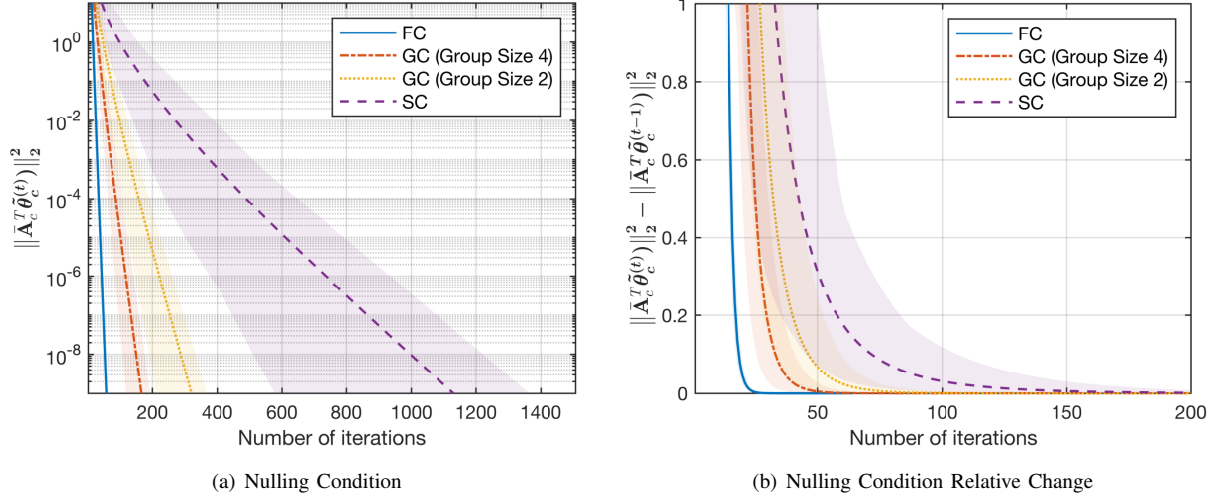


Fig. 2. Convergence of Algorithm 1 vs. number of iterations for passive interference nulling using fully-connected “FC”, group-connected “GC”, and single-connected “SC” BD-RISs with random initialization, where  $K = 8$  and  $N = 144$ . a) Nulling condition  $l^2$  norm. b) Nulling condition  $l^2$  norm relative change.

TABLE I  
SUMMARY OF THE COMPUTATIONAL AND CIRCUIT TOPOLOGY COMPLEXITIES FOR THE PROPOSED BD-RIS DESIGNS.

BD-RIS Design		Computational Complexity	Circuit Topology Complexity
Single-Connected	Passive MRT	$\mathcal{O}(KN + N)$	$N$
	Passive Interference Nulling	$\mathcal{O}(tN + K^6 + K^4N + K^2N^2 + K^2N)$	
Fully-Connected	Passive MRT	$\mathcal{O}(N^3 + KN^2 + N^2)$	$\frac{N(1+N)}{2}$
	Passive Interference Nulling	$\mathcal{O}(tN^3 + tN^2 + K^6 + K^4N^2 + K^2N^4 + K^2N^2)$	
Group-Connected	Passive MRT	$\mathcal{O}(GN_g^3 + GKN_g^2 + GN_g^2)$	$\frac{N(1+N_g)}{2}$
	Passive Interference Nulling	$\mathcal{O}(tGN_g^3 + tGN_g^2 + K^6 + K^4GN_g^2 + K^2G^2N_g^4 + K^2GN_g^2)$	

Results and Discussions Section will show that initializing based on passive MRT solution, (14), (23), improves the sum rate performance compared to the random initialization.

*Channel State Information Requirements:* The interference channels matrix  $\bar{\mathbf{A}}_c$  is needed to compute  $\Theta^*$ . This can be found by pre-designing the variation of  $\Theta$  for the single/group-connected BD-RIS architecture to be further used in the training process [35].

For the readers convenience, Table I summarizes the computational complexity and circuit topology complexity for the different BD-RIS passive MRT and passive interference nulling designs.

#### IV. STAGE 2: BS POWER ALLOCATION/PRECODING

As  $\Theta^*$  is determined at stage 1, the precoding matrix  $\mathbf{P}$  relies only on the equivalent channel matrix, i.e.,  $\mathbf{E} = \mathbf{H}\Theta^*\mathbf{W}$  which is of low-dimension compared to the individual channel matrices. Hence, (9a) can be written as

$$(P4): \max_{\mathbf{P}} \sum_k \log_2 \left( 1 + \frac{|\mathbf{h}_k^T \Theta^* \mathbf{W} \mathbf{p}_k|^2}{\sum_{i \neq k} |\mathbf{h}_k^T \Theta^* \mathbf{W} \mathbf{p}_i|^2 + N_0} \right) \quad (37a)$$

$$\text{Subject to, (9b)} \quad (37b)$$

Solving this optimization problem for the general case is not straightforward. Therefore, a distinction is made between the passive MRT and interference nulling solutions.

##### A. Power Allocation/Precoding for Passive MRT

Since the passive MRT presented in Sec. III-III-A does not set the interference terms to zero, a low-complexity precoder can be considered at the BS such as ZF. Consequently,

$$\mathbf{P} = \mathbf{E}^\dagger \sqrt{\frac{P_{\max}}{\text{Tr}(\mathbf{E}^\dagger \mathbf{H} \mathbf{E})}} \quad (38)$$

where the normalization factor ensures  $\|\mathbf{P}\|_F^2 = P_{\max}$ . The computational complexity of the ZF solution is bounded by the dimension of the equivalent channels matrix, and hence, it can be written as  $\mathcal{O}(K^3)$ .

Alternatively, employing simple power allocation approaches at the BS will ease the requirements of high resolution digital-to-analog converters [36]. In addition, the number of real variables will reduce to  $K$ , unlike the full precoder which has  $K^2$  complex variables. Two power allocation approaches are devised, which are the uniform power and optimized power. The former considers equal power allocation among the signal vector elements, i.e.,

$$\mathbf{P} = \text{diag}(\sqrt{p_1}, \sqrt{p_2}, \dots, \sqrt{p_K}) \quad (39)$$

such that  $p_k = \frac{P_{\max}}{K}$ ,  $\forall k$ . Hence, it is agnostic to the equivalent channels matrix. On the other hand, while the equivalent channels matrix is known at the BS, the optimized power can be designed to maximize the sum rate of the system. Therefore,

the sum rate maximization problem can be formulated as [37, Eq. (3)],

$$(P5): \max_{p_k} \sum_k \log_2 \left( 1 + \frac{p_k |\mathbf{h}_k^T \boldsymbol{\Theta}^* \mathbf{w}_k|^2}{\sum_{i \neq k} p_i |\mathbf{h}_k^T \boldsymbol{\Theta}^* \mathbf{w}_i|^2 + N_0} \right) \quad (40a)$$

$$\text{Subject to,} \quad \sum_k p_k = P_{\max} \quad (40b)$$

$$p_k \geq 0 \quad (40c)$$

where (40a) is non-linear and non-convex, (40b) is affine and linear and (40c) defines a hyperplane and is convex. Such optimization problem can be solved efficiently using interior-point optimization algorithms.

### B. Power Allocation for Passive Interference Nulling

Since the passive interference nulling presented in Sec. III-III-B achieves ZF when sufficient number of REs exist, i.e.,  $N \geq \left\lceil \frac{4K(K-1)}{1+N_g} \right\rceil$ ,  $\mathbf{E}$  is a diagonal matrix. Hence, the transmission results in  $K$  virtual parallel streams. Therefore, full precoding is not required to maximize the sum rate. Alternatively, water-filling power allocation can be used, which is optimal for (40a). The closed-form water-filling solution is given as

$$p_k^* = \left( \frac{1}{\alpha} - \frac{N_0}{|\mathbf{h}_k^T \boldsymbol{\Theta}^* \mathbf{w}_k|^2} \right)^+ \quad (41)$$

where  $\alpha$  is the dual variable that can be found using bi-section search. It is worth noting that the water-filling solution for passive interference nulling converges to the uniform power solution at high signal to noise ratios (SNRs), unlike passive MRT which still requires power allocation/precoding at the BS. Hence, in the presence of imperfect CSI at high SNRs, passive interference nulling is more robust as CSI is only required at the BD-RIS, compared to passive MRT which requires CSI at the BS and BD-RIS.

## V. NUMERICAL RESULTS AND DISCUSSIONS

This section presents the numerical results for the proposed two-stage designs as well as the benchmarks.

### A. Simulation Setup

The adopted channel model is i.i.d Rayleigh fading with the distance-dependent large-scale fading given as  $\Upsilon(d) = C_0 \left( \frac{d}{d_0} \right)^{-\rho}$ , where  $d$  denotes the distance,  $C_0 = -30$  dB denotes the reference pathloss,  $d_0 = 1$  m is reference distance and  $\rho = 2.2$  is the pathloss exponent. We consider the system to be operating at 2.4 GHz, with noise power spectral density  $N_0 = -80$  dBm that is identical for all users. Unless otherwise stated, we consider the distance between BS and BD-RIS to be 50 m and the distance between the BD-RIS and users to be 2.5 m. We assume the channel state information to be known perfectly at the BS, BD-RIS and the users. For Algorithm 1,  $\epsilon = 10^{-6}$ ,  $\varepsilon = 10^{-6}$  and  $\text{Iter} = 10^2$  are set. Hundred realizations are considered for Monte-Carlo simulation. The simulations were conducted on a work station equipped with 3.49 GHz 64 bits Apple M2 Pro chip with 12-core CPU and 16 GB RAM.

### B. Notations for Proposed Designs and Benchmarks

Various *benchmarks* are used to compare the performance of our *proposed* designs for the BD-RIS. The notations for the stage 1 *proposed* designs are given as follows:

- **MRT** denotes the passive MRT solution introduced in Sec. III-III-A.
- **Null** denotes the passive interference nulling introduced in Sec. III-III-B, where MRT initializations (14), (23) are considered for Algorithm 1.

The notations for the stage 2 processes at the BS are:

- **ZF** denotes the zero-forcing precoder shown in (38).
- **UP** denotes the uniform power allocation shown in (39).
- **RM** denotes the rate maximization optimization (P5) shown in (40a)–(40c) and the closed-form water-filling shown in (41).

The considered *benchmarks* are:

- **Joint** denotes the joint-design for the BD-RIS following [17], which has a computational complexity of  $\mathcal{O}(t_1 t_2 t_3 G N_g^3)$  for the group-connected, where  $t_1, t_2$  and  $t_3$  are the number of iterations for the algorithm loops.
- **Max-F** denotes the Frobenius norm-based maximum channel gain design for the BD-RIS scattering matrix. It aims to  $\max_{\boldsymbol{\Theta}} \|\mathbf{E}\|_F^2$ , which has a relaxed closed-form solution that follows [34]. The optimal solution that belongs to  $\mathcal{S}_{\text{SC}_1}$  and  $\mathcal{S}_{\text{SC}_2}$  for the single-connected is given as

$$[\boldsymbol{\Theta}^*]_{i,j} = \begin{cases} \Pi_{\mathcal{S}_{\text{unim}}}([\mathbf{v}_{\max}]_i), & i = j \\ 0, & i \neq j \end{cases} \quad (42)$$

where  $\mathbf{v}_{\max}$  is the Eigenvector of  $\mathbf{A}_c^H \mathbf{A}_c$  associated with its dominant Eigenvalue. The optimal solution that belongs to  $\mathcal{S}_{\text{GC}_1}$  and  $\mathcal{S}_{\text{GC}_2}$  for the group-connected is given as (22) and

$$\boldsymbol{\Theta}_g^* = \Pi_{\mathcal{S}_{\text{symuni}}} \left( \text{unvec} \left( \sqrt{N_g} \mathbf{v}_{g,\max}, [N_g, N_g] \right) \right) \quad (43)$$

where  $\mathbf{v}_{g,\max} = [\mathbf{v}_{\max}]_{(g-1)N_g^2+1:gN_g^2}$ . Its computational complexity comes from computing SVD for  $G N_g^2 \times G N_g^2$  matrix and is  $\mathcal{O}(G^3 N_g^6)$ . At the BS, ZF is performed following (38), which has a computational complexity of  $\mathcal{O}(K^3)$  that comes from computing the Moore-pseudoinverse of  $\mathbf{E}$ .

- **Spec-ZF** denotes the the specular reflection by BD-RIS, i.e.,  $\boldsymbol{\Theta}^* = \mathbf{I}$ , where the BS performs ZF based on  $\mathbf{E}$  such that  $\mathbf{P} = \mathbf{E}^\dagger \sqrt{\frac{P_{\max}}{\text{Tr}(\mathbf{E}^\dagger \mathbf{E})}}$  and has a computational complexity of  $\mathcal{O}(K^3)$ .
- **Spec-MRT** denotes the the specular reflection by BD-RIS, i.e.,  $\boldsymbol{\Theta}^* = \mathbf{I}$ , where the BS performs MRT based on  $\mathbf{E}$  such that  $\mathbf{P} = \mathbf{E}^H \sqrt{\frac{P_{\max}}{\text{Tr}(\mathbf{E}^H \mathbf{E})}}$  and has a computational complexity of  $\mathcal{O}(K^2)$ .

### C. Simulation Results

Fig. 3 illustrates the received SINR at stage 1 of a fully-connected and group-connected BD-RISs with  $K = 5$ , comparing relaxed and symmetric unitary solutions for **MRT** and **Max-F**. Specifically, the figure breakdowns (11) into the sum

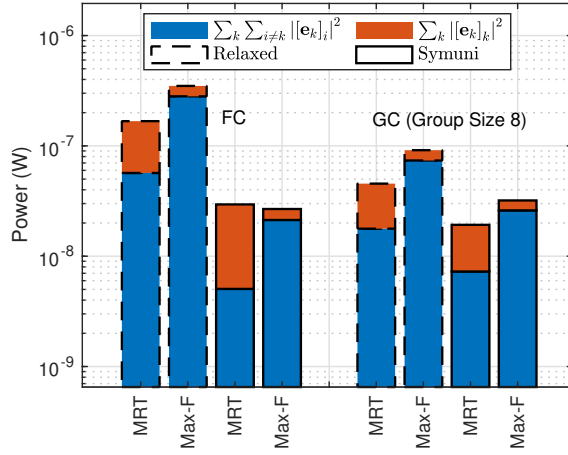


Fig. 3. Desired and interference powers for fully-connected “FC” and group-connected “GC” BD-RIS considering **MRT** and **Max-F** for  $p_k = 1, \forall k$ ,  $K = 5$  and  $N = 16$ .

of desired signals’ powers and sum of interference signals’ powers for  $N = 16$  in a stacked bar chart. It is seen that the relaxed **Max-F** achieves the highest Frobenius norm having the highest bar. Nonetheless, the symmetric unitary solution for **Max-F** does not guarantee the maximization of the Frobenius norm as seen for the fully-connected case, where the symmetric unitary **MRT** is better. In addition, the sum of desired signals’ powers for the relaxed and symmetric unitary **MRT** are higher than that of **Max-F** as expected, whereas the sum of interference signals’ powers is higher for **Max-F** compared to **MRT** as the latter only maximizes the diagonal entries of the equivalent channel but the former maximizes all entries. Such observation indicates that **MRT** would have a better SINR at the users compared to **Max-F**. Furthermore, although the SVD-based symmetric unitary projection degrades the sum of desired signals’ powers for both **Max-F** and **MRT**, it reduces the sum of interference signals’ powers for **MRT** at a higher rate such that the SINR can be effectively improved, unlike **Max-F** which reduces both the sum of signal powers and sum of interference at the same rate.

Fig. 4 compares the sum rate performance of interference nulling using single/group/fully-connected BD-RISs. The system uses MRT initialization and uniform power allocation at the BS, with  $K = 5$  and  $N \in \{32, 64\}$ <sup>1</sup>. As shown in Fig. 4a, the fully-connected BD-RIS outperforms the single-connected BD-RIS for both  $N = 32$  and  $N = 64$  with a huge gap. This performance gap is linked to the fully-connected BD-RIS requiring fewer REs to effectively null the interference with high probability. Specifically, (33) shows that the fully-connected BD-RIS requires  $N \geq 2K - 1$ , while the single-connected BD-RIS needs  $N \geq 2K(K - 1)$ . Furthermore, Fig. 4b shows that increasing the number of users, while fixing the number of REs, does not necessarily improve the sum rate. For instance, when  $N$  is sufficiently large, the fully-connected BD-RIS has an improved sum rate as more users are served. This occurs because, when  $N \gg 2K - 1$ , inter-

ference is nulled successfully using the required  $2K - 1$  REs, leaving a substantial portion of the remaining REs to enhance the signal power. In contrast, both the group-connected and single-connected BD-RISs show a degraded sum rate as the number of users increases. This degradation arises because  $N$  is not sufficiently large to achieve  $N \gg 2K(K - 1)$  and  $N \gg \left\lceil \frac{4K(K-1)}{1+N_g} \right\rceil$ . Consequently, most of the REs are used to null the interference, i.e.,  $2K(K - 1)$  and  $\left\lceil \frac{4K(K-1)}{1+N_g} \right\rceil$  REs, leaving only a small portion of REs to enhance the signal power.

Fig. 5 shows the sum rate of single/group/fully-connected BD-RISs as a function of transmit power at the BS. It considers the *proposed* BD-RIS designs, specifically considering the **MRT** and **Null** schemes. Additionally, the impact of different stage 2 processes at the BS is considered. The highlighted scenario in the figure is  $K = 5$  users and  $N = 64$  REs. Focusing on **UP**, Fig. 5 shows that **MRT** outperforms **Null** at low SNRs, where performance is primarily dominated by noise. This is because **MRT** provides a better channel alignment compared to **Null**. However, at moderate and high SNRs, **MRT** becomes interference-limited leading its performance to saturate, unlike **Null**, which inherently eliminates the interference. On the other hand, **RM** power allocation schemes improve the sum rate of **MRT** in general. While **RM** also enhances the sum rate of **Null** at low SNRs, the improvement at high SNRs is negligible. Finally, considering the fully-connected BD-RIS as an example, **MRT** with **ZF** precoding at the BS outperforms **Null** with **RM** at the BS by 1.3 dB at 20 bps/Hz. Thus, **MRT** with **ZF** at the BS achieves a balance between low computational complexity and good sum rate performance at low and moderate SNRs, while offering the best sum rate performance at high SNRs.

Fig. 6 presents the sum rate performance for both the *proposed* designs and the *benchmarks* across single/group/fully-connected BD-RISs, where  $P_{\max} = 5$  dBm. In Fig. 6a, the sum rate is illustrated as a function of number of users, where  $N = 2K(K - 1)$  REs. It can be seen that **Joint** serves as an upper bound, with the gap between the upper bound and the *proposed* designs varying based on the BD-RIS architecture. For instance, the gap is extremely tight for the fully-connected BD-RIS since  $N \gg 2K - 1$ , meaning that  $N$  is sufficiently large compared to the bound in (33). In contrast, the group-connected and single-connected BD-RISs exhibit a much larger gap from the upper bound, as  $N$  is not sufficiently large when compared to the bound in (33). For instance, at  $K = 8$ , the fully-connected BD-RIS with **Joint** achieves a sum rate of 28.3 bps/Hz, whereas **MRT** with **ZF** at the BS achieves a sum rate of 27.7 bps/Hz<sup>2</sup>. Additionally, both *proposed* BD-RIS designs outperform **Max-F** designs because the *proposed* BD-RIS designs have better interference management in multiuser systems. In addition, **Spec-ZF** and **Spec-MRT** are both performing poorly, particularly for the fully-connected BD-RIS. This is because these designs fail to leverage the BD-RIS to mitigate the poor channel gains caused by the double-fading effect, making reliance on the BS solely

<sup>1</sup>Note that uniform power allocation is not optimal to maximize the sum rate. Nonetheless, it is considered in this figure to assess the sum rate performance of passive interference nulling using BD-RIS.

<sup>2</sup>It is worth noting that **Joint** only considers (9d) constraint, while the rest BD-RIS designs consider both (9c) and (9d) constraints.

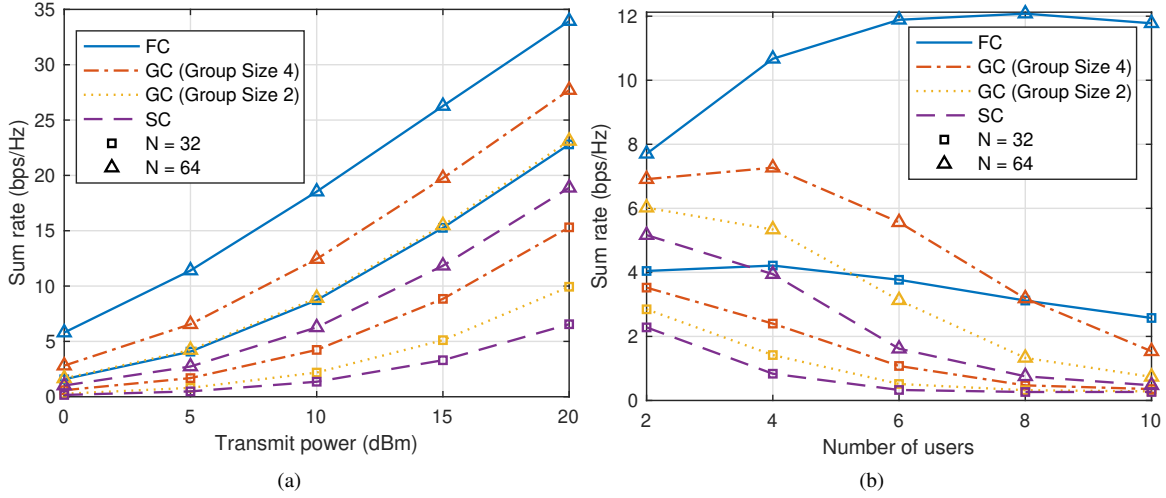


Fig. 4. Sum rate for passive interference nulling using fully-connected “FC”, group-connected “GC”, and single-connected “SC” BD-RISs with MRT initialization, where a) x-axis is transmit power and  $K = 5$ . b) x-axis is number of users and  $P_{\max} = 5$  dBm.

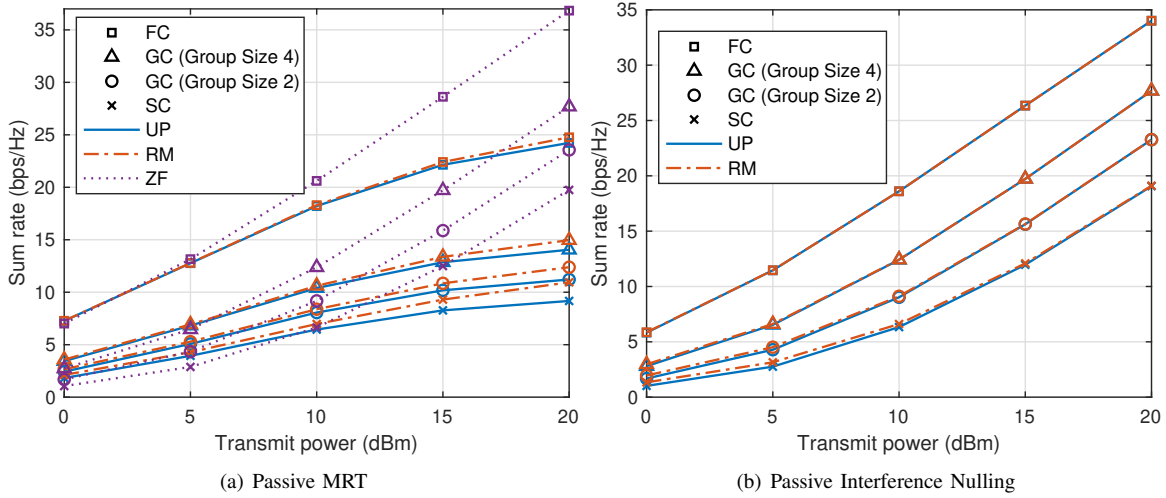


Fig. 5. Sum rate vs. transmit power for the stage 2 processes at the BS using fully-connected “FC”, group-connected “GC”, and single-connected “SC” BD-RISs, where  $K = 5$ ,  $P_{\max} = 5$  dBm,  $N = 64$ . a) Passive MRT. b) Passive interference nulling.

for precoding inefficient. For instance, ZF wastes most of the power for channel inversion leaving very small power gains. Moreover, the performance of the *proposed* designs improve as the number of users/REs increase which is justified by the growing Frobenius norm of the scattering matrix, indicating their effectiveness in handling dense multiuser scenarios. While the gap between **MRT** and **Null** with MRT initialization increases as the number of users increase, the latter can be a good candidate to achieve a reasonable sum rate performance meanwhile maintaining a negligible complexity at the BS.

Furthermore, Fig. 6b shows the sum rate as a function of number of REs for  $K = 2$ . It is seen that **Joint** serves as an upper bound here too, where the gap between the upper bound and the *proposed* designs is very tight given that the range of  $N$  is sufficiently large for all BD-RIS architectures given  $K = 2$ . This indicates that passive MRT with ZF precoding at the BS achieves local optimality while maintaining low complexity, and is considered a good candidate for BD-RIS with many REs. The specular reflection **BD-RIS** curves on the

other hand are both lower bounds and the justification holds from Fig. 6a. Also, the significance of **Max-F** is shown for high number of REs. Their poor performance with relatively small  $N$  is justified by the fact that the equivalent channel is ill-conditioned/poorly conditioned for such  $N$  values and it improves as  $N$  increases.

Fig. 7 shows the computational complexity considering the *proposed* designs and *benchmarks* for single/group/fully-connected, where  $K = 2$ . The worst-case scenario is considered for **Joint** and **Null** with MRT initialization, such that  $t_1 = 50$ ,  $t_2 = 20$ ,  $t_3 = 5$ , and  $t = 100$ . As presented in Table I and Sec. V-V-B, **MRT** has the lowest time complexity while the **Max-F** has the highest. Although **Joint** has a cubic time complexity, the complexity from the iterative algorithm is not negligible. Furthermore, **Null** has a lower complexity compared to both *benchmarks*.

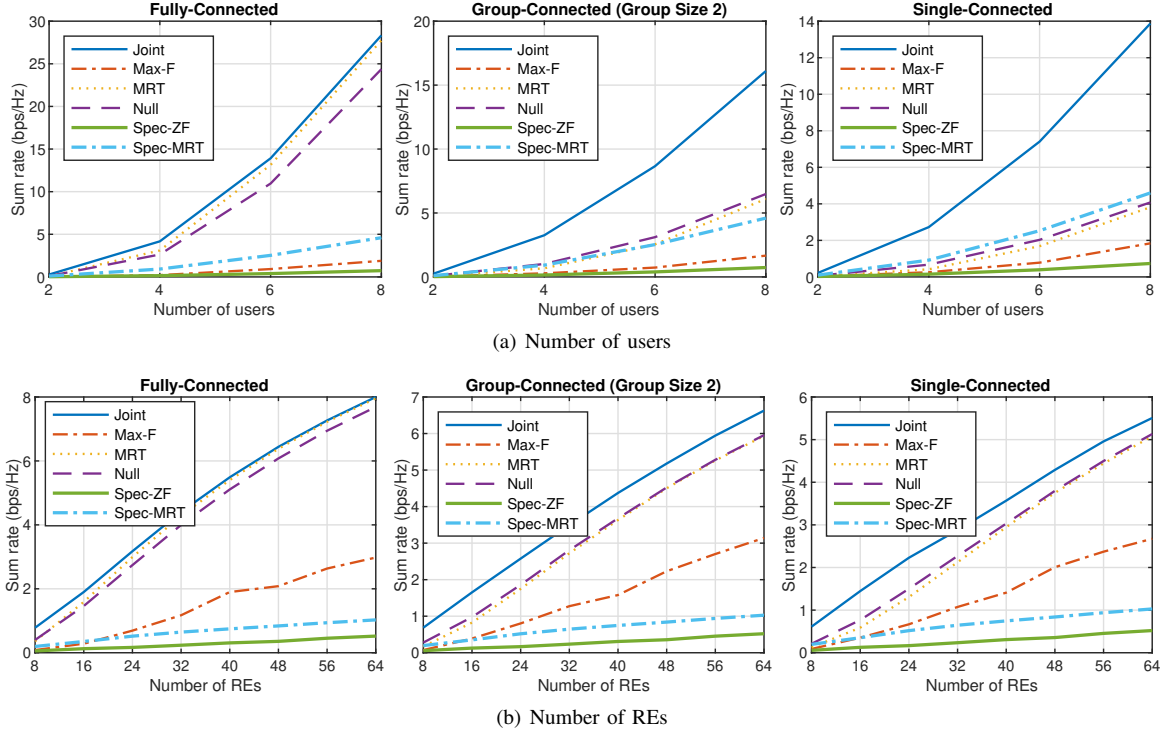


Fig. 6. Sum rate for the *benchmarks* and *proposed* designs for fully-connected, group-connected and single-connected BD-RISs with  $P_{\max} = 5$  dBm. a) x-axis is number of users,  $N = 2K(K - 1)$ . b) x-axis is number of REs,  $K = 2$ .

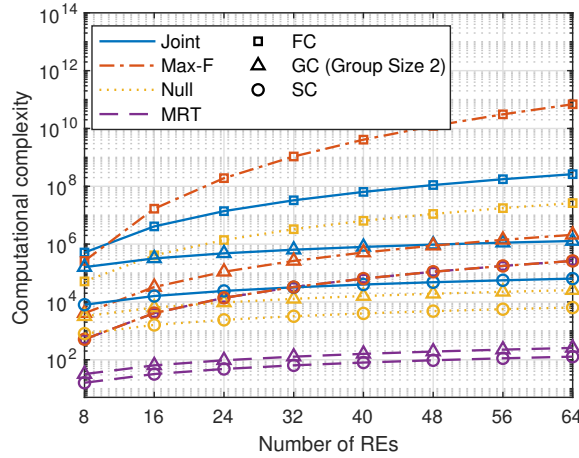


Fig. 7. Computational complexity as a function of number of REs. The *proposed* designs and *benchmarks* are considered for fully-connected “FC”, group-connected “GC” and single-connected “SC” BD-RISs, where  $K = 2$ .

## VI. CONCLUSIONS AND FUTURE WORK

To conclude, this work proposed a passive multiuser beamforming for single/group/fully-connected BD-RIS-enabled MU-MISO systems. The passive multiuser beamforming designs are inspired by MRT and interference nulling. The former passive beamforming is presented in closed-form while the latter is presented in an AO framework. At the BS side, optimized/uniform power allocation and active precoding are considered. It is seen that the fully-connected BD-RIS reduces the number of REs required to achieve interference nulling and achieves faster convergence compared to D-RIS. In addition, the passive MRT at BD-RIS with ZF precoding at the BS

presents an effective low-complexity solution that simplifies channel estimation and achieves local optimality for MU-MISO scenarios with many REs.

For the future work, we will consider deriving a closed-form unitary symmetric scattering matrix to achieve *interference nulling* for the BD-RIS. In addition, we will analyze the average SINR and outage probability for the *passive MRT*. An extension to multi-antenna users will also be considered. Furthermore, we will generalize the BD-RIS scattering matrix design and BS precoder design to account for the imperfect CSI.

## REFERENCES

- [1] M. Di Renzo *et al.*, “Smart radio environments empowered by reconfigurable intelligent surfaces: How it works, state of research, and the road ahead,” *IEEE J. Sel. Areas Commun.*, vol. 38, no. 11, pp. 2450–2525, Nov. 2020.
- [2] —, “Reconfigurable intelligent surfaces vs. relaying: Differences, similarities, and performance comparison,” *IEEE Open J. Commun. Soc.*, vol. 1, pp. 798–807, Jun. 2020.
- [3] J. An, C. Xu, L. Gan, and L. Hanzo, “Low-complexity channel estimation and passive beamforming for RIS-assisted MIMO systems relying on discrete phase shifts,” *IEEE Trans. Commun.*, vol. 70, no. 2, pp. 1245–1260, Feb. 2022.
- [4] Y. Liu *et al.*, “Reconfigurable intelligent surfaces: Principles and opportunities,” *IEEE Commun. Surveys Tuts.*, vol. 23, no. 3, pp. 1546–1577, 3rd Quart. 2021.
- [5] E. Björnson *et al.*, “Reconfigurable intelligent surfaces: A signal processing perspective with wireless applications,” *IEEE Signal Process. Mag.*, vol. 39, no. 2, pp. 135–158, Feb. 2022.
- [6] Q. Wu and R. Zhang, “Intelligent reflecting surface enhanced wireless network via joint active and passive beamforming,” *IEEE Trans. Wireless Commun.*, vol. 18, no. 11, pp. 5394–5409, Nov. 2019.
- [7] Z. Yang, W. Xu, C. Huang, J. Shi, and M. Shikh-Bahaei, “Beamforming design for multiuser transmission through reconfigurable intelligent surface,” *IEEE Trans. Commun.*, vol. 69, no. 1, pp. 589–601, Jan. 2021.

- [8] Q.-U.-A. Nadeem *et al.*, “Intelligent reflecting surface-assisted multi-user MISO communication: Channel estimation and beamforming design,” *IEEE Open J. Commun. Soc.*, vol. 1, pp. 661–680, May 2020.
- [9] Y. Liu, L. Zhang, and M. A. Imran, “Multi-user beamforming and transmission based on intelligent reflecting surface,” *IEEE Trans. Wireless Commun.*, vol. 21, no. 9, pp. 7329–7342, Sep. 2022.
- [10] T. Jiang and W. Yu, “Interference nulling using reconfigurable intelligent surface,” *IEEE J. Sel. Areas Commun.*, vol. 40, no. 5, pp. 1392–1406, May 2022.
- [11] F. Zhu *et al.*, “Robust beamforming for RIS-aided communications: Gradient-based manifold meta learning,” *arXiv preprint arXiv:2402.10626*, 2024.
- [12] S. Jangsher, M. Al-Jarrah, A. Al-Dweik, E. Alsusa, and P.-Y. Kong, “Energy constrained sum-rate maximization in IRS-assisted UAV networks with imperfect channel information,” *IEEE Trans. Aerosp. Electron. Syst.*, vol. 59, no. 3, pp. 2898–2908, Jun. 2023.
- [13] S. Shen, B. Clerckx, and R. Murch, “Modeling and architecture design of reconfigurable intelligent surfaces using scattering parameter network analysis,” *IEEE Trans. Wireless Commun.*, vol. 21, no. 2, pp. 1229–1243, Feb. 2022.
- [14] H. Li, S. Shen, M. Nerini, and B. Clerckx, “Reconfigurable intelligent surfaces 2.0: Beyond diagonal phase shift matrices,” *IEEE Commun. Mag.*, vol. 62, no. 3, pp. 102–108, Mar. 2024.
- [15] M. Nerini, S. Shen, H. Li, and B. Clerckx, “Beyond diagonal reconfigurable intelligent surfaces utilizing graph theory: Modeling, architecture design, and optimization,” *IEEE Trans. Wireless Commun.*, pp. 1–1, 2024.
- [16] H. Li, S. Shen, and B. Clerckx, “Beyond diagonal reconfigurable intelligent surfaces: From transmitting and reflecting modes to single-, group-, and fully-connected architectures,” *IEEE Trans. Wireless Commun.*, vol. 22, no. 4, pp. 2311–2324, Apr. 2023.
- [17] —, “Beyond diagonal reconfigurable intelligent surfaces: A multi-sector mode enabling highly directional full-space wireless coverage,” *IEEE J. Sel. Areas Commun.*, vol. 41, no. 8, pp. 2446–2460, Aug. 2023.
- [18] Y. Zhou, Y. Liu, H. Li, Q. Wu, S. Shen, and B. Clerckx, “Optimizing power consumption, energy efficiency, and sum-rate using beyond diagonal ris—a unified approach,” *IEEE Trans. Wireless Commun.*, vol. 23, no. 7, pp. 7423–7438, Jul. 2024.
- [19] M. Nerini, S. Shen, and B. Clerckx, “Closed-form global optimization of beyond diagonal reconfigurable intelligent surfaces,” *IEEE Trans. Wireless Commun.*, vol. 23, no. 2, pp. 1037–1051, Feb. 2024.
- [20] W. Sun, S. Sun, T. Shi, X. Su, and R. Liu, “A new model of beyond diagonal reconfigurable intelligent surfaces (BD-RIS) for the corresponding quantization and optimization,” *IEEE Trans. Wireless Commun.*, vol. 23, no. 9, pp. 11 521–11 534, Sep. 2024.
- [21] T. Fang and Y. Mao, “A low-complexity beamforming design for beyond-diagonal RIS aided multi-user networks,” *IEEE Commun. Lett.*, vol. 28, no. 1, pp. 203–207, Jan. 2024.
- [22] T. D. Hua, M. Mohammadi, H. Q. Ngo, and M. Matthaiou, “Cell-free massive MIMO SWIPT with beyond diagonal reconfigurable intelligent surfaces,” in *IEEE Wireless Commun. Netw. Conf. (WCNC)*, Dubai, UAE, Jul. 2024, pp. 1–6.
- [23] Z. Liu, Y. Liu, S. Shen, Q. Wu, and Q. Shi, “Enhancing ISAC network throughput using beyond diagonal RIS,” *IEEE Wireless Commun. Lett.*, vol. 13, no. 6, pp. 1670–1674, Jun. 2024.
- [24] K. Chen and Y. Mao, “Transmitter side beyond-diagonal RIS for mmWave integrated sensing and communications,” *arXiv preprint arXiv:2404.12604*, 2024.
- [25] Q. Li *et al.*, “Reconfigurable intelligent surfaces relying on non-diagonal phase shift matrices,” *IEEE Trans. Veh. Technol.*, vol. 71, no. 6, pp. 6367–6383, Jun. 2022.
- [26] Q. Li, M. El-Hajjar, I. Hemadeh, A. Shojaeifard, and L. Hanzo, “Coordinated reconfigurable intelligent surfaces: Non-diagonal group-connected design,” *IEEE Trans. Veh. Technol.*, vol. 73, no. 7, pp. 10 811–10 816, Jul. 2024.
- [27] Y. Dong, Q. Li, S. X. Ng, and M. El-Hajjar, “Reconfigurable intelligent surface relying on low-complexity joint sector non-diagonal structure,” *IEEE Open J. Veh. Technol.*, vol. 5, pp. 1106–1123, Aug. 2024.
- [28] I. Santamaria, M. Soleymani, E. Jorswieck, and J. Gutiérrez, “SNR maximization in beyond diagonal RIS-assisted single and multiple antenna links,” *IEEE Signal Process. Lett.*, vol. 30, pp. 923–926, 2023.
- [29] R. Zhang, C. C. Chai, and Y.-C. Liang, “Joint beamforming and power control for multiantenna relay broadcast channel with QoS constraints,” *IEEE Trans. Signal Process.*, vol. 57, no. 2, pp. 726–737, Feb. 2009.
- [30] E. Björnson, M. Bengtsson, and B. Ottersten, “Optimal multiuser transmit beamforming: A difficult problem with a simple solution structure [lecture notes],” *IEEE Signal Process. Mag.*, vol. 31, no. 4, pp. 142–148, Jul. 2014.
- [31] T. Lo, “Maximum ratio transmission,” *IEEE Trans. Commun.*, vol. 47, no. 10, pp. 1458–1461, Oct. 1999.
- [32] X. Tang and Y. Hua, “Optimal design of non-regenerative MIMO wireless relays,” *IEEE Trans. Wireless Commun.*, vol. 6, no. 4, pp. 1398–1407, Apr. 2007.
- [33] E. Björnson, D. Hammarwall, and B. Ottersten, “Exploiting quantized channel norm feedback through conditional statistics in arbitrarily correlated MIMO systems,” *IEEE Trans. Signal Process.*, vol. 57, no. 10, pp. 4027–4041, Oct. 2009.
- [34] O. T. Demir and E. Björnson, “Is channel estimation necessary to select phase-shifts for RIS-assisted massive MIMO?” *IEEE Trans. Wireless Commun.*, vol. 21, no. 11, pp. 9537–9552, Nov. 2022.
- [35] H. Li, S. Shen, Y. Zhang, and B. Clerckx, “Channel estimation and beamforming for beyond diagonal reconfigurable intelligent surfaces,” *IEEE Trans. Signal Process.*, vol. 72, pp. 3318–3332, 2024.
- [36] J. An, M. Di Renzo, M. Debbah, and C. Yuen, “Stacked intelligent metasurfaces for multiuser beamforming in the wave domain,” in *IEEE Int. Conf. Commun. (IEEE ICC)*, Rome, Italy, 2023, pp. 2834–2839.
- [37] C. Huang, A. Zappone, G. C. Alexandropoulos, M. Debbah, and C. Yuen, “Reconfigurable intelligent surfaces for energy efficiency in wireless communication,” *IEEE Trans. Wireless Commun.*, vol. 18, no. 8, pp. 4157–4170, Aug. 2019.